SCIENCE CHINA
Technological Sciences

•Article•

April 2020 Vol.63 No.4: 603–613
https://doi.org/10.1007/s11431-019-1450-6

Memristor initial-boosted coexisting plane bifurcations and its extreme multi-stability reconstitution in two-memristor-based dynamical system

BAO Han, CHEN Mo, WU HuaGan & BAO BoCheng*

School of Information Science and Engineering, Changzhou University, Changzhou 213164, China

Received July 30, 2019; accepted September 30, 2019; published online November 19, 2019

Initial-dependent extreme multi-stability and offset-boosted coexisting attractors have been significantly concerned recently. This paper constructs a novel five-dimensional (5-D) two-memristor-based dynamical system by introducing two memristors with cosine memductance into a three-dimensional (3-D) linear autonomous dissipative system. Through theoretical analyses and numerical plots, the memristor initial-boosted coexisting plane bifurcations are found and the memristor initial-dependent extreme multi-stability is revealed in such a two-memristor-based dynamical system with plane equilibrium. Furthermore, a dimensionality reduction model with the determined equilibrium is established via an integral transformation method, upon which the memristor initial-dependent extreme multi-stability is reconstituted theoretically and expounded numerically. Finally, physically circuit-implemented PSIM (power simulation) simulations are carried out to validate the plane offset-boosted coexisting behaviors.

memristor-based system, memristor initial, coexisting plane bifurcations, extreme multi-stability

Citation: Bao H, Chen M, Wu H G, et al. Memristor initial-boosted coexisting plane bifurcations and its extreme multi-stability reconstitution in two-memristor-based dynamical system. Sci China Tech Sci, 2020, 63: 603–613, https://doi.org/10.1007/s11431-019-1450-6

1 Introduction

Due to the nonlinearity, plasticity, and non-volatile memory [1], numerous memristor-based chaotic oscillating circuits and neuromorphic computing circuits have been broadly developed in the past few years. Generally regarded as nonlinear components, memristors can be conveniently introduced into various pre-existing oscillation circuits to trigger chaotic oscillations. Some specific dynamical behaviors, such as self-exited hyperchaotic oscillations [2–4], hidden chaotic or hyperchaotic oscillations [5,6], coexisting multiple attractors [7,8], infinitely many coexisting attractors [9–11], transient hyperchaotic oscillations [12,13], and chaotic and periodic bursting oscillations [14,15], were disclosed by theoretical analyses, numerical simulations, and/or hardware experiments. Interestingly enough, memristors can be utilized to mimic neural synapses in biological neurons [16–18] and to characterize the effects of electromagnetic induction/radiation [19–22]. By employing the pinched hysteresis loops, power-off plot, and dynamic route map, Rajamani et al. [23] validated the calcium and potassium ion-channels in Morris-Lecar neuron model of the third-order barnacle muscle fiber as generic and volatile memristors. Based on the presented memristor crossbar-based neuromorphic computing system, Hu et al. [24] investigated the recall and training functions of the character recognition process with multi-answer. By utilizing the voltage-controlled memristor model, Ntinas et al. [25] developed a digitally circuit-implemented memristor emulator for synthesizing memristor-based oscillation circuits and de-

*Corresponding author (email: mervinbao@126.com)

ploying synapse functions in artificial neural networks. In brief, memristors with the synaptic plasticity and non-volatile memory are increasingly becoming the promising candidates for neuromorphic computing circuits [26–31].

With the small size and low power consumption, memristor-based chaotic oscillating circuits and neuromorphic computing circuits have widely potential application prospects [10,32]. Careful dynamical analyses of these memristor-based application circuits exhibit that the memristor initials do play an especially important role in complex dynamics of these circuits [33,34]. Usually, ideal memristor-based oscillating circuits are extremely easy to generate infinitely many coexisting attractors, resulting in the emergence of initial-dependent extreme multi-stability [35–37]. The phenomenon of initial-dependent extreme multi-stability relates to the ideal memristor-based oscillating circuits owning infinitely many line or plane equilibrium points [4,10–12], no equilibrium point [38], or switchable no and line equilibrium point [39]. Therefore, an effective approach to generate infinitely many coexisting attractors is to introduce one, two, or more ideal memristors into some pre-existing circuits and systems. In contrast, another useful approach to generate infinitely many initial-offset boosted attractors is to introduce periodic trigonometric functions in some specific offset-boostable chaotic systems [40–44]. Offset boosting associates with a variable transformation that shifts any of the variables in a dynamical system such that its phase space attractor does not alter the system solutions [40]. If the periods for all the periodic trigonometric functions are the same, any phase space attractor will be infinitely copied by periodic offset boosting [42]. In both approaches, the attractor offset-boosted behaviors are achieved by changing the initials. However, the ideal memristor-based oscillating circuits generally possess complete bifurcation routes with the initial evolutions [10], which allow more attractor types to be coined in these circuits.

Motivated by these two approaches, this paper presents a novel five-dimensional (5-D) two-memristor-based dynamical system, which is yielded by introducing two memristors with cosine memductance into a three-dimensional (3-D) linear system. Although the presented two-memristor-based dynamical system has the forms of periodic trigonometric functions, the nonlinear terms are the product of the cosine functions and the state variables, in which these cosine functions can be regarded as two alterable system parameters controlled by other state variables. As expected, the memristor initial-dependent bifurcation boosting behaviors and infinite plane offset-boosted coexisting attractors are uncovered in such a two-memristor-based dynamical system. In fact, combining the two approaches can be a very effective way to implement the initial offset-boosted coexisting plane bifurcations with more complex extreme multi-stability, which has not yet clarified previously.

2 Two-memristor-based system with plane equilibrium

Memristor is a nonlinear electronic component. A novel memristor with cosine memductance is considered firstly, which is described as

$$\begin{aligned} i_M &= W(\varphi)v_M = \cos(\varphi)v_M, \\ \dot{\varphi} &= v_M, \end{aligned} \tag{1}$$

where v_M and i_M represent the input voltage and output current, respectively. Thus, the memductance can be expressed by

$$W(\varphi) = \cos(\varphi). \tag{2}$$

The cosine memductance is periodically multi-valued, which is different from the quadratic double-valued memductance utilized in [2,3,12] and threshold single-valued memductance reported in [21,39]. As a sinusoidal stimulus is applied, the presented memristor exhibits the property of pinched hysteresis loops by numerical and circuit simulations.

By introducing two nonlinear memristors described in eq. (1) into a 3-D linear autonomous dissipative system, a novel 5-D two-memristor-based dynamical system is easily constructed, which is modeled by

$$\begin{aligned} \dot{x} &= y + z - k\cos(v)y, \\ \dot{y} &= -x + z, \\ \dot{z} &= -x - z + k\cos(u)x, \\ \dot{u} &= x, \\ \dot{v} &= y, \end{aligned} \tag{3}$$

where the control parameter k is a positive constant. In this study, the unique parameter is kept unchanged as k=3.

Obviously, the two-memristor-based dynamical system owns a plane equilibrium, which is expressed as

$$S = \{(x,y,z,u,v) | x = y = z = 0, u = \mu, v = \eta\}, \tag{4}$$

where μ and η are two alterable constants.

The Jacobian matrix $\mathbf{J}_{\mathrm{O}}$ for the 5-D system (eq. (3)) at the plane equilibrium S is derived as

$$\mathbf{J}_{\mathrm{O}} = \begin{bmatrix} 0 & 1-k\cos(\eta) & 1 & 0 & 0 \\ -1 & 0 & 1 & 0 & 0 \\ -1+k\cos(\mu) & 0 & -1 & 0 & 0 \\ 1 & 0 & 0 & 0 & 0 \\ 0 & 1 & 0 & 0 & 0 \end{bmatrix}. \tag{5}$$

Thus, the characteristic polynomial equation is yielded as

$$P_{\mathrm{O}}(\lambda) = \lambda^2(\lambda^3 + a_1\lambda^2 + a_2\lambda + a_3) = 0, \tag{6}$$

where

$$a_1 = 1,$$

$$a_2 = 2 - k\cos(\mu) - k\cos(\eta),$$

$$a_3 = [2 - k\cos(\mu)][1 - k\cos(\eta)].$$

The eq. (6) illustrates that Jacobian matrix $\mathbf{J}_{\mathrm{O}}$ has two zero

roots and three non-zero roots. For the three non-zero roots, Routh-Hurwitz conditions are given by

$$a_1 > 0,\ a_3 > 0,\ \text{and}\ a_1 a_2 - a_3 > 0. \tag{7}$$

If the conditions of eq. (7) are satisfied, S is stable, leading to the existence of point attractor. In contrast, if any one of the conditions of eq. (7) is not satisfied, S is unstable, resulting in that unstable behaviors may be generated in the two-memristor-based system.

With the conditions of eq. (7), when both the memristor initials μ and η are increased from $-\pi$ to π in the primary area $(-\pi, \pi)$, different stability distributions for the three non-zero roots are colored in the μ–η initial plane, as shown in Figure 1, where USP, USF, and SNF represent unstable saddle point, unstable saddle-focus, and stable node-focus, respectively. Note that 0P3N means three negative real parts with no positive real part in the three non-zero roots, and 1P2N and 2P1N imply one and two positive real parts in the three non-zero roots. For some initials μ and η located in different colored regions, the three non-zero roots are solved from eq. (6) and the corresponding stability types can be thereby obtained, which are summarized in Table 1. Hence, complex stability distributions can be observed in the μ–η initial plane, which demonstrates that abundant dynamical behaviors are closely dependent on the two memristor initials.

3 Coexisting plane bifurcations boosted by memristor initials

Of particular concern is that the two-memristor-based dynamical system can emerge coexisting plane bifurcations through offset boosting the memristor initials. The unique control parameter is kept unchanged as k=3 and the initials are set as $(x(0), y(0), z(0), u(0), v(0))=(10^{-9}, 0, 0, \mu, \eta)$.

3.1 Mechanism analysis of coexisting plane bifurcations

By integrating the last two equations of the two-memristor-based dynamical system given in eq. (3) from $-\infty$ to τ, there yields:

$$\begin{aligned} u &= \int_{-\infty}^{\tau} x(\xi)\mathrm{d}\xi = \int_{-\infty}^{0} x(\xi)\mathrm{d}\xi + \int_{0}^{\tau} x(\xi)\mathrm{d}\xi, \\ v &= \int_{-\infty}^{\tau} y(\xi)\mathrm{d}\xi = \int_{-\infty}^{0} y(\xi)\mathrm{d}\xi + \int_{0}^{\tau} y(\xi)\mathrm{d}\xi. \end{aligned} \tag{8}$$

Define

$$\begin{aligned} \mu &= u(0) = \int_{-\infty}^{0} x(\xi)\mathrm{d}\xi, \\ \eta &= v(0) = \int_{-\infty}^{0} y(\xi)\mathrm{d}\xi, \end{aligned} \tag{9}$$

as the initials of two memristor inner state variables. Putting eq. (9) into eq. (8), these two expressions in eq. (8) are simplified as

$$\begin{aligned} u &= \mu + \int_{0}^{\tau} x(\xi)\mathrm{d}\xi, \\ v &= \eta + \int_{0}^{\tau} y(\xi)\mathrm{d}\xi. \end{aligned} \tag{10}$$

Substituting eq. (10) into eq. (3) and eliminating the nonrelevant last two equations of eq. (3), the two-memristor-based dynamical system can be then rewritten as

$$\begin{aligned} \dot{x} &= y + z - k\cos[\eta + \int_{0}^{\tau} y(\xi)\mathrm{d}\xi]y, \\ \dot{y} &= -x + z, \\ \dot{z} &= -x - z + k\cos[\mu + \int_{0}^{\tau} x(\xi)\mathrm{d}\xi]x. \end{aligned} \tag{11}$$

Thus, the two memristor initials μ and η can be explicitly expressed in eq. (11).

For two natural numbers m and n, denote

$$\begin{aligned} \mu &= \mu_0 \pm 2m\pi, \\ \eta &= \eta_0 \pm 2n\pi, \end{aligned} \tag{12}$$

where μ_0 and η_0 are two compensation initials that allow two

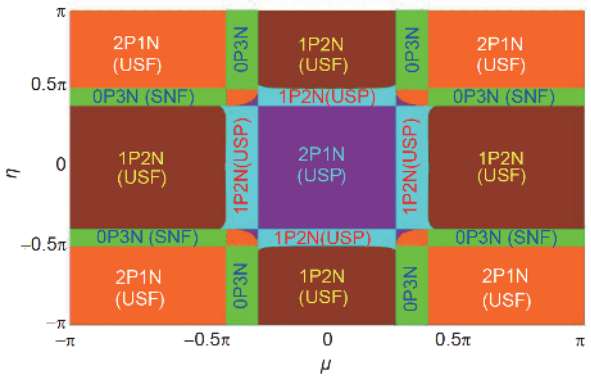

Figure 1 Stability distributions of three non-zero roots in the μ–η initial plane with k=3, where different colored regions have different stability types.

Table 1 Non-zero roots, colored regions and stability types for different initials in $(-\pi, \pi)$

μ, η	Non-zero roots	Colored regions	Stability types
0, 0	1.0000, 0.7321, −2.7321	Purple	USP (2P1N)
0, ±1.5	1.0000, −0.5393, −1.4607	Cyan	USP (1P2N)
0, ±2.5	1.0000, −1.0000 ±j1.5503	Brown	USF (1P2N)
±1, 0	1.3524, −0.2691, −2.0833	Cyan	USP (1P2N)
±1, ±1.5	0.0481±j0.5197, −1.0963	Orange	USF (2P1N)
±1, ±2.5	−0.2452±j1.5724, −0.5094	Green	SNF (0P3N)
±2, 0	1.5486, −1.2743 ±j1.6036	Brown	USF (1P2N)
±2, ±1.5	−0.0628±j1.7095, −0.8745	Green	SNF (0P3N)
±2, ±2.5	0.3231±j2.5713, −1.6463	Orange	USF (2P1N)

following relations be satisfied as

$$-\pi< \mu_0+\int_0^{\tau}x(\xi)\mathrm{d}\xi <\pi,$$
$$-\pi< \eta_0+\int_0^{\tau}y(\xi)\mathrm{d}\xi <\pi. \tag{13}$$

So that we have

$$\cos[\mu+\int_0^{\tau}x(\xi)\mathrm{d}\xi]=\cos[\mu_0+\int_0^{\tau}x(\xi)\mathrm{d}\xi],$$
$$\cos[\eta+\int_0^{\tau}y(\xi)\mathrm{d}\xi]=\cos[\eta_0+\int_0^{\tau}y(\xi)\mathrm{d}\xi]. \tag{14}$$

The above results exhibit the cyclic repetition of cosine memductance given in eq. (2).

The system model described by the mathematical equations of eq. (11) is cyclic about the two memristor initials μ and η. The cyclic characteristic can be derived from the invariance of the model (eq. (11)) when substituting the conversions in eq. (12) into eq. (11). It turns out that the bifurcation behaviors of the two-memristor-based dynamical system are cyclically varied with the periodic evolutions of the two memristor initials μ and η, so that the memristor initial regions in the μ–η plane can be divided into $m\times n$ bifurcation distribution windows that each has width 2π and height 2π. Therefore, the two-memristor-based system described by eq. (3) is a plane bifurcation-boostable system induced by the two memristor initials in the μ–η initial plane.

3.2 Coexisting plane bifurcations by numerical plots

Based on fourth-order Runge-Kutta algorithm, the time-step 0.01 and time-interval [550, 600] are employed. Firstly, the memristor initial η is set as 2π, 0, and -2π, respectively, and the memristor initial μ is varied in the region $[-3\pi, 3\pi]$. The bifurcation diagrams of the maxima $v_{\max}$ of the state variable v are together simulated, as shown in Figure 2(a), where the dark green, black and magenta colored trajectories correspond to $\eta=2\pi$, 0 and -2π, respectively. Secondly, the memristor initial μ is arranged as 3π, π, and $-\pi$, respectively, and the memristor initial η is adjusted in the region $[-3\pi, 3\pi]$. The bifurcation diagrams of the maxima $u_{\max}$ of the state variable u are together simulated, as shown in Figure 2(b), where the blue, brown and red colored trajectories relate to 3π, π, and $-\pi$, respectively.

Corresponding to the bifurcation diagrams in Figure 2, the first four Lyapunov exponents (LEs) are numerically drawn, as shown in Figure 3, from which it can be seen that the dynamics depicted by the LEs are exactly the same as those described by the bifurcation diagrams. Remark that there are always two zero LEs with the variations of the memristor initials μ and η, which are caused by the introduction of two memristors.

Observed from Figures 2 and 3, chaotic, periodic, and point behaviors with forward/reverse period-doubling bifurcation routes and crisis scenarios along with anti-monotonicity can be found, which just reflect the emergence of extreme multi-stability, i.e., the coexistence of infinitely many attractors. In particular, coexisting plane bifurcations with the identical bifurcation structure are boosted in the two

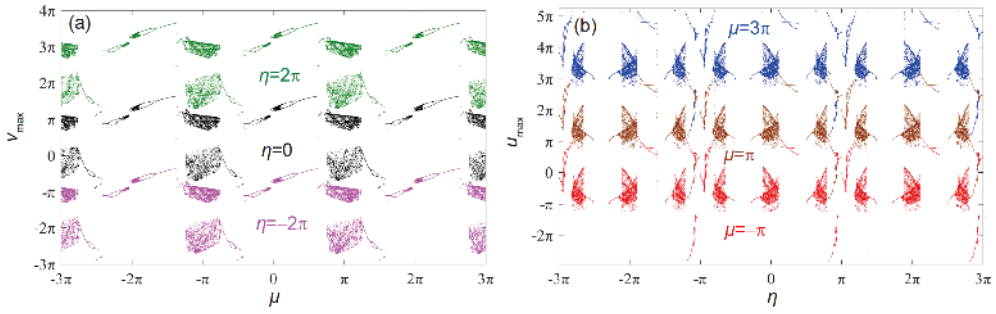

Figure 2 Initial-dependent bifurcation boosting behaviors along the v coordinate and u coordinate with the variations of the memristor initials μ and η, where $x(0)=10^{-9}$, $y(0)=0$, and $z(0)=0$. (a) For three different values of η, bifurcation diagrams as μ varies in $[-3\pi, 3\pi]$; (b) for three different values of μ, bifurcation diagrams as η varies in $[-3\pi, 3\pi]$.

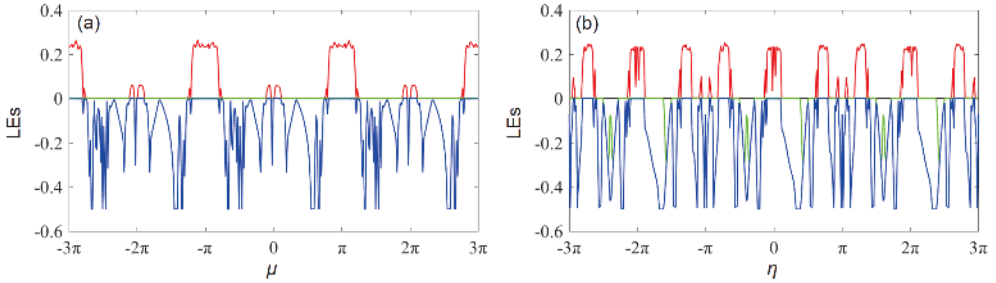

Figure 3 First four LEs corresponding to the bifurcation diagrams in Figure 2. (a) For $\eta=0$, LEs as μ varies in $[-3\pi, 3\pi]$; (b) for $\mu=\pi$, LEs as η varies in $[-3\pi, 3\pi]$.

dimension of $u\times v$ owning a width or height 2π cycle by the periodically varied memristor initials in such a two-memristor-based system, which are distinguished from those of the reported boosting behaviors in [40–44].

As shown in Figure 4, the memristor initial-offset boosting behaviors in the two dimension of $u\times v$ in system (3) can be depicted by phase plots in the u–v plane, where seven kinds of memristor initial offset-boosted coexisting attractors are disclosed. Thus, the coexisting disconnected attractors with different attractor types (such as chaos, period, and point), different attractor structures (such as double-scroll, single-scroll, large size, small size), different periodicities (such as period-1, period-2, period-4), and different positions (such as left, right, up, down) are included in Figure 4. Particularly, when m and n tend to infinite, infinitely many coexisting attractors, i.e., extreme multi-stability, are emerged in the two-memristor-based system.

The attraction basin is the initial plane region of an attractor, in which any initial point will be iterated into the attractor. Here the two memristor initials are treated two invariant measures for classification of dynamical behaviors [45,46]. Through examining the periodicities of the state variable y, 2-D attraction basin in the μ–η initial plane is plotted for the two-memristor-based system with k=3, as shown in Figure 5(a). The colored attracting regions represent the memristor initial regions that trigger the motion trajectories with different periodicities. In other words, the red marked with CH stands for chaos, the yellow marked

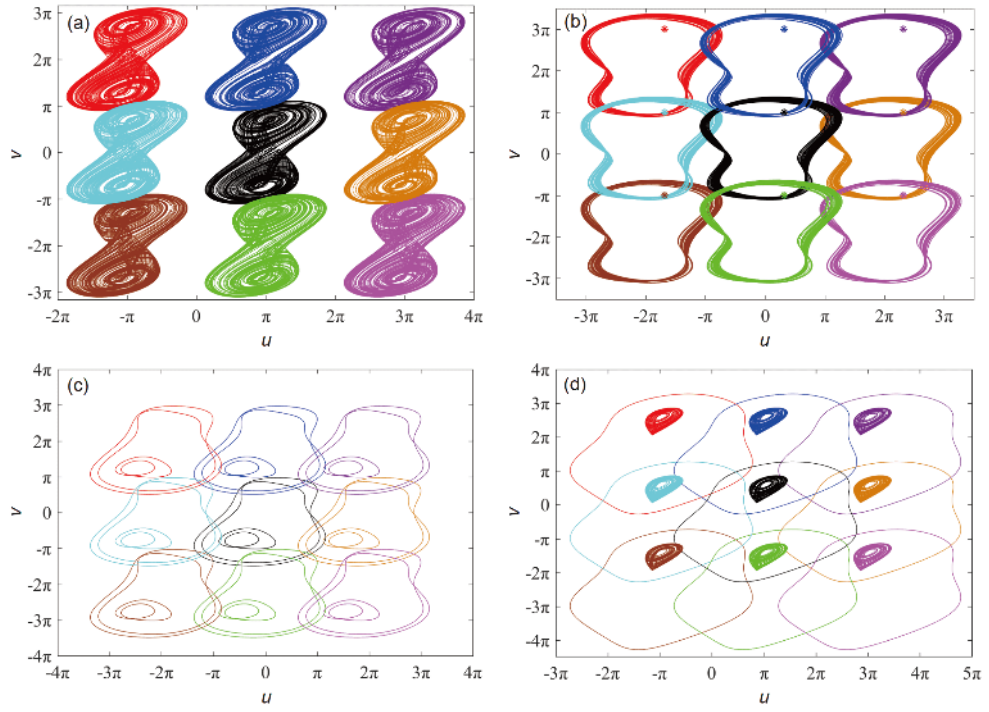

Figure 4 Memristor initial offset-boosted coexisting attractors distributed in the u–v plane, where (m, n=0, ±1). (a) Double-scroll chaotic attractors under (μ, η)=(π+2$m\pi$, 2$n\pi$); (b) single-scroll chaotic attractors under (μ, η)=(0.2+2$m\pi$, 2$n\pi$) and points under (μ, η)=(1+2$m\pi$, π+2$n\pi$); (c) large size period-2 limit cycles under (μ, η)=(−0.8+2$m\pi$, 2$n\pi$) and small size period-2 limit cycles under (μ, η)=(−1.8+2$m\pi$, 2$n\pi$); (d) chaotic spiral attractors under (μ, η)=(π+2$m\pi$, 1.98+2$n\pi$) and period-1 limit cycles under (μ, η)=(π+2$m\pi$, 1+2$n\pi$). Here black for (m, n)=(0, 0), blue for (m, n)=(0, 1), green for (m, n)=(0, −1), purple for (m, n)=(1, 1), orange for (m, n)=(1, 0), magenta for (m, n)=(1, −1), red for (m, n)=(−1, 1), cyan for (m, n)=(−1, 0), brown for (m, n)=(−1, −1).

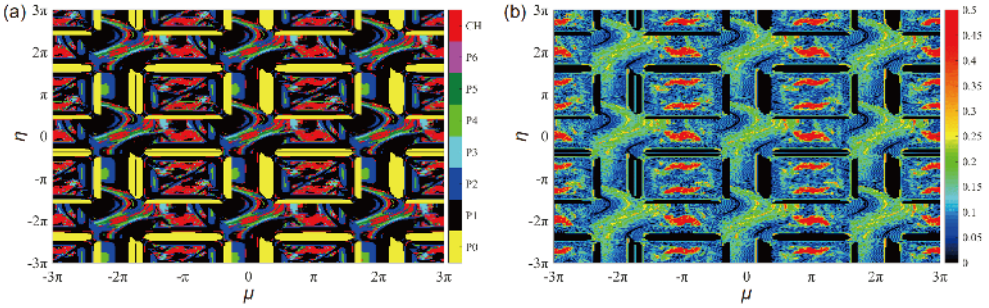

Figure 5 2-D dynamical behaviors in the μ–η initial plane. (a) Memristor initial attraction basin through examining the periodicities of the state variable y; (b) spectral entropy-based complexity for the time series of the state variable y.

with P0 denotes point, and the other colors marked with P1–P6 represent limit cycles with period-1 to period-6. Thus, abundantly memristor initial-dependent dynamical behaviors with the plane cyclic characteristic can be uncovered by the 2-D attraction basin in Figure 5(a).

To further confirm the complex dynamical behaviors triggered by the memristor initials, the complexity distributed in the μ–η initial plane for the two-memristor-based system can be calculated and drawn in Figure 5(b), where the complexity values using the rods are obtained by calculating the spectral entropy of the time series of the state variable y based on the Fourier transform [39,47]. The irregularly chaotic time series possesses a relatively large complexity value, whereas the regularly periodic time series owns a relatively small complexity value. Hence, the complexity distributions in Figure 5(b) can reflect the dynamical behaviors closely relying on the memristor initials, similar to those demonstrated in Figure 5(a).

The numerical plots given in Figure 5 effectively validate the plane cyclic characteristic for the two memristor initials μ and η. In each of the cyclic areas, a variety of disconnected attractors can be intuitively exhibited in Figure 5, including chaotic attractors with different topologies, limit cycles with different periodicities, and stable points with different positions. Therefore, the phenomenon of memristor initial-dependent extreme multi-stability, i.e., the coexistence of infinitely many disconnected attractors, is demonstrated in the two-memristor-based system.

4 Extreme multi-stability reconstitution via integral transformation

An integral transformation method [11,34] can be applied to derive the dimensionality reduction model of system (3). By doing so, all the system initials are converted into the initial-related parameters in an explicit form. Thus, the memristor initial-motivated extreme multi-stability in the original system is reconstituted by the initial parameter-associated dynamics of the dimensionality reduction model.

4.1 Dimensionality reduction model with determined equilibrium

To employ the integral transformation method in [11,34], five new state variables X, Y, Z, U, and V for representing the incremental integral transformation of the original state variables x, y, z, u, and v are defined as

$$\begin{aligned} &X(\tau)=\int_0^\tau x(\xi)\mathrm{d}\xi,\ Y(\tau)=\int_0^\tau y(\xi)\mathrm{d}\xi,\\ &Z(\tau)=\int_0^\tau z(\xi)\mathrm{d}\xi,\ U(\tau)=\int_0^\tau u(\xi)\mathrm{d}\xi,\\ &V(\tau)=\int_0^\tau v(\xi)\mathrm{d}\xi, \end{aligned} \tag{15}$$

and the five system initials are denoted as

$$c_1=x(0),\ c_2=y(0),\ c_3=z(0),\ \mu=u(0),\ \eta=v(0), \tag{16}$$

where μ and η are two alterable constants.

By integrating the equations of eq. (3) from 0 to τ and considering the definitions of eq. (15), one has:

$$\begin{aligned} &x-x(0)=Y+Z-k\int_0^\tau \cos[v(\xi)]y(\xi)\mathrm{d}\xi,\\ &y-y(0)=-X+Z,\\ &z-z(0)=-X-Z+k\int_0^\tau \cos[u(\xi)]x(\xi)\mathrm{d}\xi,\\ &u-u(0)=X,\\ &v-v(0)=Y. \end{aligned} \tag{17}$$

Based on the last two equations of eq. (3), there exists the relations $\mathrm{d}u(\tau)=x(\tau)\mathrm{d}\tau$ and $\mathrm{d}v(\tau)=y(\tau)\mathrm{d}\tau$, so that the integral terms in eq. (17) are formulated as

$$\begin{aligned} \int_0^\tau \cos[u(\xi)]x(\xi)\mathrm{d}\xi &= \int_0^\tau \cos[u(\xi)]\mathrm{d}u(\xi)\\ &= \sin[u(\tau)]-\sin[u(0)]\\ &= \sin(X+\mu)-\sin(\mu), \end{aligned} \tag{18a}$$

$$\begin{aligned} \int_0^\tau \cos[v(\xi)]y(\xi)\mathrm{d}\xi &= \int_0^\tau \cos[v(\xi)]\mathrm{d}v(\xi)\\ &= \sin[v(\tau)]-\sin[v(0)]\\ &= \sin(Y+\eta)-\sin(\eta). \end{aligned} \tag{18b}$$

Meanwhile, according to the definitions of eq. (15), the original state variables can be expressed by the reconstituted state variables as

$$\begin{aligned} &x(\tau)=\frac{\mathrm{d}X(\tau)}{\mathrm{d}\tau},\ y(\tau)=\frac{\mathrm{d}Y(\tau)}{\mathrm{d}\tau},\ z(\tau)=\frac{\mathrm{d}Z(\tau)}{\mathrm{d}\tau},\\ &u(\tau)=\frac{\mathrm{d}U(\tau)}{\mathrm{d}\tau},\ v(\tau)=\frac{\mathrm{d}V(\tau)}{\mathrm{d}\tau}. \end{aligned} \tag{19}$$

Substituting eqs. (16), (18) and (19) into eq. (17), a mathematical model with the reconstituted state variables and five initial-related parameters are derived as

$$\begin{aligned} &\dot{X}=Y+Z-k\sin(Y+\eta)+k\sin(\eta)+c_1,\\ &\dot{Y}=-X+Z+c_2,\\ &\dot{Z}=-X-Z+k\sin(X+\mu)-k\sin(\mu)+c_3,\\ &\dot{U}=X+\mu,\\ &\dot{V}=Y+\eta. \end{aligned} \tag{20}$$

Since the last two equations of eq. (20) have nothing to do with the first three equations, the model eq. (20) can be simplified by

$$\begin{aligned} &\dot{X}=Y+Z-k\sin(Y+\eta)+k\sin(\eta)+c_1,\\ &\dot{Y}=-X+Z+c_2,\\ &\dot{Z}=-X-Z+k\sin(X+\mu)-k\sin(\mu)+c_3, \end{aligned} \tag{21}$$

where the explicitly appearing parameters c_1, c_2, c_3, μ, and η stand for the initials of the original system (3).

The newly reconstituted model (21) is a 3-D dimensionality reduction system with the initial-related parameters in an explicit form, which can be employed for quantitatively exploring the initial-dependent dynamics of the two-

memristor-based system. Consequently, the extreme multi-stability disclosed in system (3) can be reconstituted by the initial parameter-associated dynamics in the dimensionality reduction model (21). Note that the model initials of (21) are ensured to be set as $X(0)=Y(0)=Z(0)=0$.

The equilibrium of the model (21) is determined by solving the following equations:

$$\begin{aligned} 0 &= Y+Z-k\sin(Y+\eta)+k\sin(\eta)+c_1, \\ 0 &= -X+Z+c_2, \\ 0 &= -X-Z+k\sin(X+\mu)-k\sin(\mu)+c_3, \end{aligned} \tag{22}$$

which can be expressed as

$$E=(\xi_1,\ \xi_2,\ \xi_1-c_2). \tag{23}$$

The ξ_1 and ξ_2 are the solutions of the following transcendental functions:

$$F_1(\xi_1)=2\xi_1-k\sin(\xi_1+\mu)+k\sin(\mu)-c_2-c_3=0, \tag{24}$$

and

$$F_2(\xi_2)=\xi_1+\xi_2-k\sin(\xi_2+\eta)+k\sin(\eta)+c_1-c_2=0, \tag{25}$$

respectively. The two functions imply that the determined equilibrium (23) depends on the five initial-related parameters c_1, c_2, c_3, μ, and η in eq. (16). Thus, the plane equilibrium S in eq. (4) can be converted into the determined equilibrium E in eq. (23).

The Jacobian matrix $\mathbf{J}_D$ for the dimensionality reduction model (21) at the determined equilibrium E is given as

$$\mathbf{J}_D=\begin{bmatrix} 0 & 1-k\cos(\xi_2+\eta) & 1 \\ -1 & 0 & 1 \\ -1+k\cos(\xi_1+\mu) & 0 & -1 \end{bmatrix}. \tag{26}$$

So that the characteristic polynomial equation is derived as

$$P_D(\lambda)=\lambda^3+b_1\lambda^2+b_2\lambda+b_3=0, \tag{27}$$

where

$$b_1=1,$$

$$b_2=2-k\cos(\xi_1+\mu)-k\cos(\xi_2+\eta),$$

$$a_3=[2-k\cos(\mu)][1-k\cos(\eta)].$$

Denote the three non-memristor initial-related parameters (c_1, c_2, c_3) as (0, 0, 0). The equilibrium of the model (21) can be numerically solved as E=(0, 0, 0). Thus, the characteristic polynomial equation given in eq. (27) is exactly the same as those of three non-zero roots in the bracket of eq. (6), resulting in the identical stability distributions in the μ–η plane. However, since the determined equilibrium E changes with the three non-memristor initial-related parameters, the stability distributions in the μ–η plane will also change.

4.2 Initial parameter-associated extreme multi-stability

Similarly, the fourth-order Runge-Kutta algorithm with the time-step and time-interval used in Figure 2 are utilized for numerically exploring the reconstituted model (21). When the initial-related parameter η is set as 0 and μ is varied in the region $[-3\pi, 3\pi]$, the bifurcation diagram of the maxima Y_{max} of the state variable Y and the first two LEs are plotted, as shown in Figure 6(a). In the same way, when the initial-related parameter μ is set as π and η is varied in the region $[-3\pi, 3\pi]$, the bifurcation diagram of the maxima X_{max} of the state variable X and the first two LEs are plotted, as shown in Figure 6(b). The numerical results in Figure 6 do well match with those in Figures 2 and 3, which manifest that the model (21) is suitable and feasible to reconstitute the memristor initial-motivated extreme multi-stability in the original system. However, the bifurcation boosting behaviors along the u coordinate and v coordinate no longer exist in the reconstituted model (21) due to the elimination of the original state variables u and v via integral transformation.

The three non-memristor initial-related parameters are set as (c_1, c_2, c_3)=(10^{-9}, 0, 0). When both the two memristor initial-related parameter μ and η are continuously altered in the region $[-3\pi, 3\pi]$, 2-D bifurcation diagram and dynamical map in the μ–η plane are shown in Figure 7(a) and (b), respectively. The 2-D bifurcation diagram in Figure 7(a) is depicted by the periodicities of the state variable Y, similar to that used in Figure 5(a). In contrast, the 2-D dynamical map in Figure 7(b) is depicted by the values of the largest LE with the coded colors [46], in which the yellow-red-white stands for positive values (chaos), the dark-yellow for zero (period), and the black for negative values (point). Therefore, the 2-D dynamical map in Figure 7(b) is a useful supplement to dynamical descriptions of the 2-D bifurcation diagram in Figure 7(a). It is observed that both complex dynamical behaviors depicted by the 2-D bifurcation diagram and dynamical map are mutually consistent, which well confirms the 2-D dynamical behaviors given in Figure 5(a), indicating the reconstitution of extreme multi-stability for the two-memristor-based dynamical system.

Furthermore, the three non-memristor initial-related parameters (c_1, c_2, c_3) are set as (1, 0, 0) and (0, 1, 0), respectively. When both the two memristor initial-related parameters μ and η are continuously altered in the region $[-3\pi, 3\pi]$, the 2-D bifurcation diagrams in the μ–η plane are shown in Figure 8. Comparing Figure 8 with Figure 7(a), the stable point regions shrink distinctly, the period-1 region enlarges apparently, and the other regions vary slightly. As a result, the non-memristor initial-related parameters (c_1, c_2, c_3) have a great impact on dynamical behaviors of the reconstituted model (21) due to the variations of the determined equilibrium and its stabilities, but the cyclically and symmetrically dynamical behaviors can be observed in the μ–η initial plane as well.

5 Physically circuit-implemented PSIM simulations

By employing operation amplifier, multiplier, capacitor,

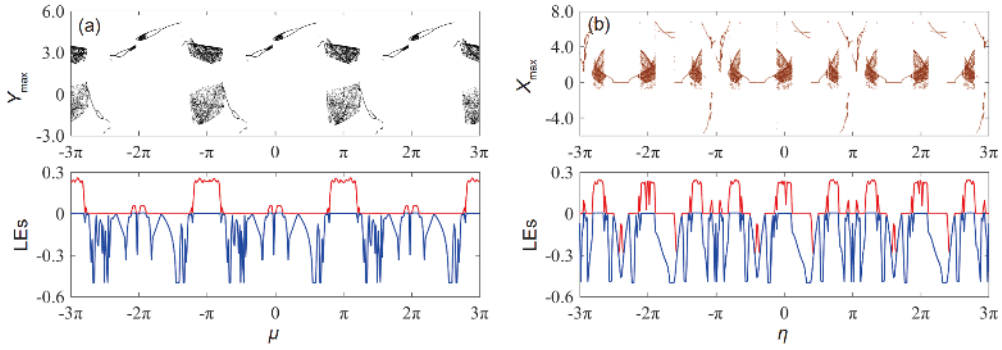

Figure 6 Numerical plots of the bifurcation diagrams and first two LEs for different bifurcation parameters. (a) For η=0, the initial-related parameter μ varying in [−3π, 3π]; (b) for μ=π, the initial-related parameter η varying in [−3π, 3π].

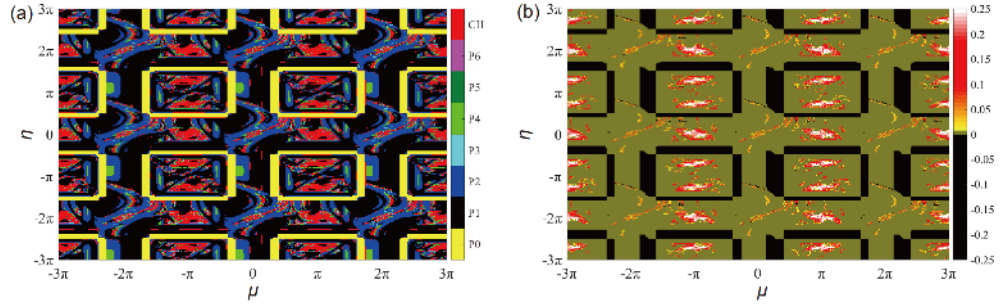

Figure 7 2-D initial-related parameter bifurcation diagram and dynamical map in the μ–η plane with (c_1, c_2, c_3)=(10^{-9}, 0, 0). (a) Bifurcation diagram depicted by the periodicities of the state variable Y; (b) dynamical map depicted by the values of the largest LE.

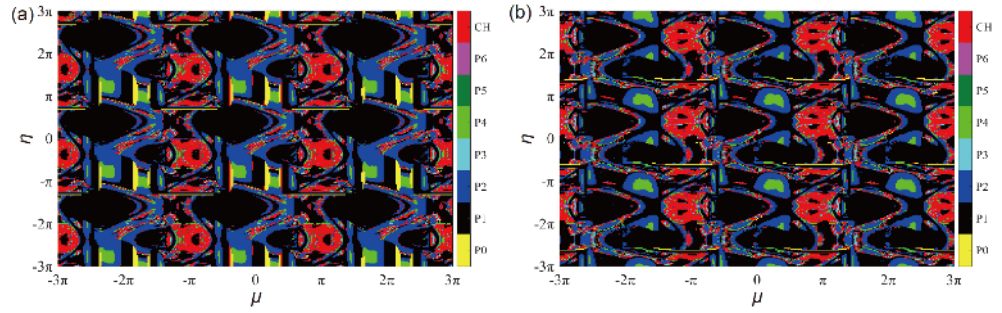

Figure 8 2-D initial-related parameter bifurcation diagrams depicted by the periodicities of the state variable Y in the μ–η plane with (a) (c_1, c_2, c_3)=(1, 0, 0) and (b) (c_1, c_2, c_3)=(0, 1, 0), demonstrating dynamical effects of the non-memristor initial-related parameters on the extreme multi-stability.

resistor, and trigonometric function converter, an analog circuit for implementing the two-memristor-based system described by eq. (3) can be designed [46,48–51]. Because the memristor initials, i.e., the initial capacitor voltages, are hardly set in hardware experiments [46,52], memristor initial plane offset-boosted coexisting attractors are confirmed by PSIM (power simulation) simulations.

Figure 9(a) displays an electronic emulator module for implementing the memristor with cosine memductance, which contains integrator U_1 (time constant τ_0=RC), trigonometric function converter U_2, multiplier U_3, and output resistor R_k. Note that the voltage output of U_2 is cos(v_φ) when choosing AD639AD as the trigonometric function converter in the physical circuit. According to the circuit schematic, the memristor emulator can be modeled as

$$\begin{aligned} i_M &= g\cos(v_\varphi)v_M / R_k, \\ RC\,\mathrm{d}v_\varphi / \mathrm{d}t &= v_M, \end{aligned} \tag{28}$$

where v_φ denotes the output voltage of integrator U_1, and g stands for the gain of multiplier U_3.

With the designed memristor emulator module, Figure 9(b) exhibits the implementation circuit of the two-memristor-based system, which only involves three integrators and three inverters. Thus, the circuit equations of the im-

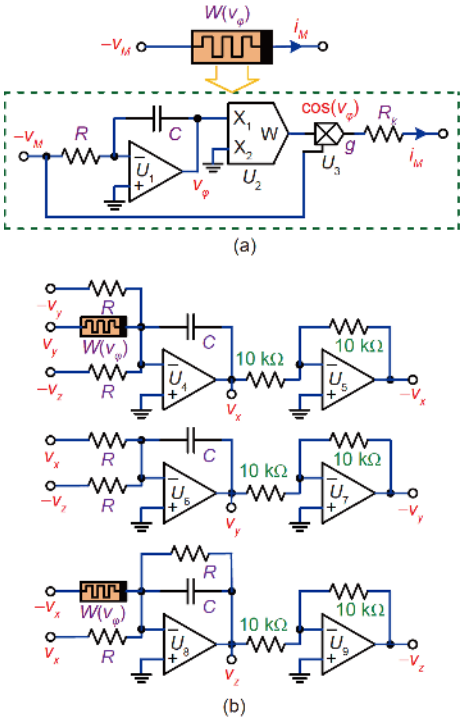

Figure 9 Circuit implementation for the two-memristor-based system. (a) Memristor emulator module; (b) analog electronic circuit.

plementation circuit shown in Figure 9 are modeled as

$$\begin{aligned}
\tau_0 \mathrm{d}v_x/\mathrm{d}t &= v_y + v_z - gR\cos(v_v)v_y/R_k,\\
\tau_0 \mathrm{d}v_y/\mathrm{d}t &= -v_x + v_z,\\
\tau_0 \mathrm{d}v_z/\mathrm{d}t &= -v_x - v_z + gR\cos(v_u)v_x/R_k,\\
\tau_0 \mathrm{d}v_u/\mathrm{d}t &= v_x,\\
\tau_0 \mathrm{d}v_v/\mathrm{d}t &= v_y,
\end{aligned} \tag{29}$$

where v_x, v_y, v_z, v_u, and v_v are the five circuit variables, $\tau_0=RC$ is the time constant of the five integrators, and g is the multiplier gain. Setting $\tau_0=RC$=15 kΩ×33 nF=495 μs and g=1, the unique circuit parameter in Figure 9 is determined as R_k=5 kΩ.

Corresponding to the phase plots in Figure 4, PSIM simulated memristor initial offset-boosted coexisting attractors distributed in the v_u–v_v plane are obtained, as shown in Figure 10. Due to the calculation errors in MATLAB numerical simulations and PSIM circuit simulations, the two memristor initials used in Figure 10 are partially different from those used in Figure 4 and period-1 limit cycles in Figure 10(d) have larger size than those in Figure 4(d). But the circuit simulated results figure out that the plane offset-boosted coexisting behaviors can be captured from the physical circuit of the two-memristor-based system as well.

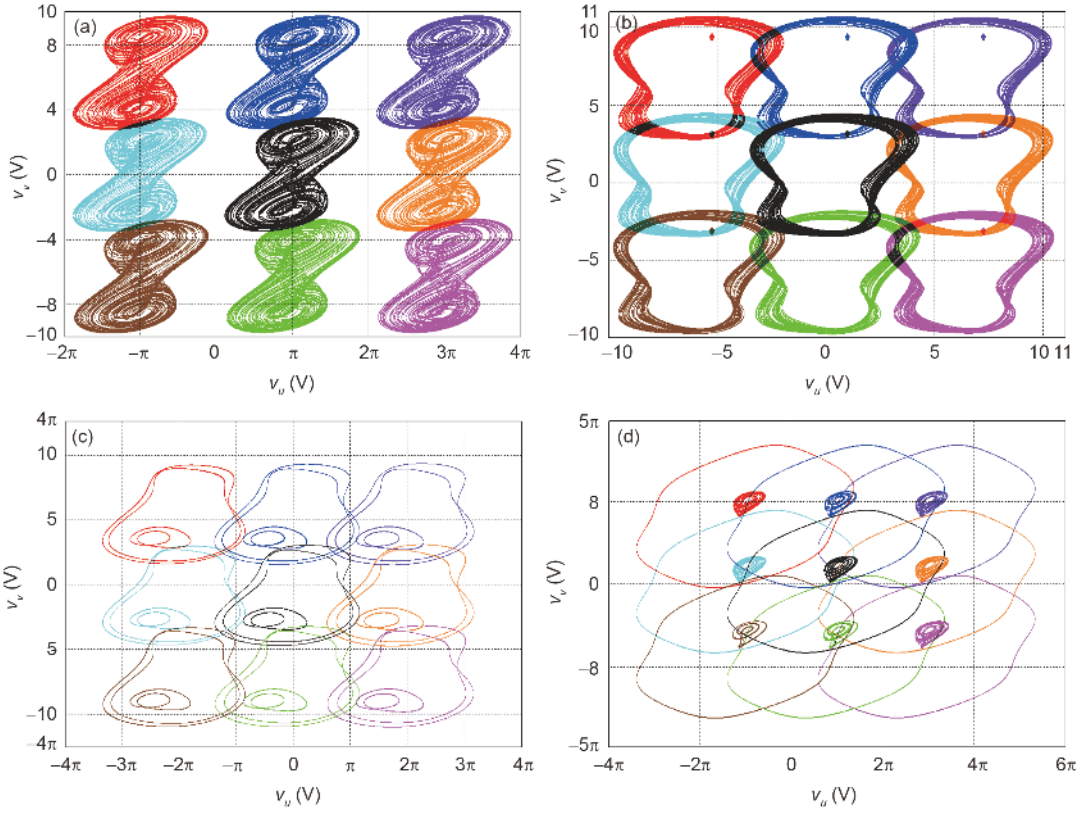

Figure 10 PSIM simulated memristor initial offset-boosted coexisting attractors distributed in the v_u–v_v plane, where (m, n=0, ±1). (a) Double-scroll chaotic attractors under (μ, η)=(π+2mπ, 2nπ); (b) single-scroll chaotic attractors under (μ, η)=(0.2+2mπ, 2nπ) and points under (μ, η)=(1+2mπ, −π+2nπ); (c) large size period-2 limit cycles under (μ, η)=(−0.8+2mπ, 2nπ) and small size period-2 limit cycles under (μ, η)=(−1.8+2mπ, 2+2nπ); (d) chaotic spiral attractors under (μ, η)=(π+2mπ, −1.98+2nπ) and period-1 limit cycles under (μ, η)=(π+2mπ, 1+2nπ). The colors coded for (m, n) represent the different values used in Figure 4.

6 Conclusions

By introducing two ideal memristors with cosine memductance into a 3-D linear autonomous system, this paper presented a novel 5-D two-memristor-based dynamical system. Thus, the two-memristor-based system was achieved by combining the two approaches to the memristor initial-motivated and periodic offset-boosted infinitely many coexisting attractors, which have been significantly concerned in plenty of research achievements recently. With the presented two-memristor-based dynamical system, the plane equilibrium and complex stability distributions in the initial plane were investigated. In the meantime, the mechanism analysis of coexisting plane bifurcations was performed, which demonstrated that the presented dynamical system was a plane bifurcation-boostable system induced by the two memristor initials. By means of numerical simulations, the memristor initial-boosted coexisting plane bifurcations were found and the memristor initial-dependent extreme multi-stability was revealed. Moreover, by using an integral transformation method, a 3-D dimensionality reduction model with the determined equilibrium was established, with which the memristor initial-dependent extreme multi-stability was reconstituted theoretically and expounded numerically. At last, physically circuit-implemented PSIM simulations were carried out to validate the plane offset-boosted coexisting behaviors. Therefore, the theoretical and numerical results prove that the initial offset-boosted coexisting plane bifurcations in the two-memristor-based system lead to the emergence of more complex extreme multi-stability, which could gain broad interest for its potential chaos-based applications by supplying more flexibility [53,54].

This work was supported by the National Natural Science Foundation of China (Grant Nos. 51777016, 51607013, 61601062 & 61801054).

1 Eshraghian K, Kavehei O, Cho K R, et al. Memristive device fundamentals and modeling: Applications to circuits and systems simulation. Proc IEEE, 2012, 100: 1991–2007
2 Li Q, Hu S, Tang S, et al. Hyperchaos and horseshoe in a 4D memristive system with a line of equilibria and its implementation. Int J Circ Theor Appl, 2014, 42: 1172–1188
3 Zhou L, Wang C, Zhou L. Generating four-wing hyperchaotic attractor and two-wing, three-wing, and four-wing chaotic attractors in 4D memristive system. Int J Bifurcation Chaos, 2017, 27: 1750027
4 Bao B, Jiang T, Wang G, et al. Two-memristor-based Chua's hyperchaotic circuit with plane equilibrium and its extreme multi-stability. Nonlinear Dyn, 2017, 89: 1157–1171
5 Prousalis D A, Volos C K, Stouboulos I N, et al. Hyperchaotic memristive system with hidden attractors and its adaptive control scheme. Nonlinear Dyn, 2017, 90: 1681–1694
6 Pham V T, Jafari S, Vaidyanathan S, et al. A novel memristive neural network with hidden attractors and its circuitry implementation. Sci China Tech Sci, 2016, 59: 358–363
7 Njitacke Z T, Kengne J, Fotsin H B, et al. Coexistence of multiple attractors and crisis route to chaos in a novel memristive diode bidge-based Jerk circuit. Chaos Soliton Fract, 2016, 91: 180–197
8 Xu Q, Zhang Q L, Qian H, et al. Crisis-induced coexisting multiple attractors in a second-order nonautonomous memristive diode bridge-based circuit. Int J Circ Theor Appl, 2018, 46: 1917–1927
9 Corinto F, Forti M. Memristor circuits: Bifurcations without parameters. IEEE Trans Circuits Syst I, 2017, 64: 1540–1551
10 Chen M, Sun M, Bao H, et al. Flux-charge analysis of two-memristor-based Chua's circuit: Dimensionality decreasing model for detecting extreme multistability. IEEE Trans Ind Electron, 2019, doi: 10.1109/TIE.2019.2907444
11 Zhang Y, Liu Z, Wu H, et al. Two-memristor-based chaotic system and its extreme multistability reconstitution via dimensionality reduction analysis. Chaos Soliton Fract, 2019, 127: 354–363
12 Bao B C, Shi G D, Xu J P, et al. Dynamics analysis of chaotic circuit with two memristors. Sci China Tech Sci, 2011, 54: 2180–2187
13 Ishaq Ahamed A, Lakshmanan M. Nonsmooth bifurcations, transient hyperchaos and hyperchaotic beats in a memristive Murali-Lakshmanan-Chua circuit. Int J Bifurcation Chaos, 2013, 23: 1350098
14 Bao B C, Wu P Y, Bao H, et al. Numerical and experimental confirmations of quasi-periodic behavior and chaotic bursting in third-order autonomous memristive oscillator. Chaos Soliton Fract, 2018, 106: 161–170
15 Wu H, Ye Y, Chen M, et al. Extremely slow passages in low-pass filter-based memristive oscillator. Nonlinear Dyn, 2019, 97: 2339–2353
16 Sah M P, Hyongsuk Kim M P, Chua L O. Brains are made of memristors. IEEE Circuits Syst Mag, 2014, 14: 12–36
17 Ma W, Zidan M A, Lu W D. Neuromorphic computing with memristive devices. Sci China Inf Sci, 2018, 61: 060422
18 Ma J, Tang J. A review for dynamics in neuron and neuronal network. Nonlinear Dyn, 2017, 89: 1569–1578
19 Bao H, Hu A H, Liu W B, et al. Hidden bursting firings and bifurcation mechanisms in memristive neuron model with threshold electromagnetic induction. IEEE Trans Neural Netw Learn Syst, 2019, doi: 10.1109/TNNLS.2019.2905137
20 Ge M, Jia Y, Xu Y, et al. Mode transition in electrical activities of neuron driven by high and low frequency stimulus in the presence of electromagnetic induction and radiation. Nonlinear Dyn, 2018, 91: 515–523
21 Bao H, Liu W, Hu A. Coexisting multiple firing patterns in two adjacent neurons coupled by memristive electromagnetic induction. Nonlinear Dyn, 2019, 95: 43–56
22 Lu L L, Jia Y, Xu Y, et al. Energy dependence on modes of electric activities of neuron driven by different external mixed signals under electromagnetic induction. Sci China Tech Sci, 2019, 62: 427–440
23 Rajamani V, Kim H, Chua L. Morris-Lecar model of third-order barnacle muscle fiber is made of volatile memristors. Sci China Inf Sci, 2018, 61: 060426
24 Hu M, Li H, Chen Y, et al. Memristor crossbar-based neuromorphic computing system: A case study. IEEE Trans Neural Netw Learn Syst, 2014, 25: 1864–1878
25 Ntinas V, Vourkas I, Abusleme A, et al. Experimental study of artificial neural networks using a digital memristor simulator. IEEE Trans Neural Netw Learn Syst, 2018, 29: 5098–5110
26 Du L, Cao Z L, Lei Y M, et al. Electrical activities of neural systems exposed to sinusoidal induced electric field with random phase. Sci China Tech Sci, 2019, 62: 1141–1150
27 Bao B, Hu A, Bao H, et al. Three-dimensional memristive hindmarsh-rose neuron model with hidden coexisting asymmetric behaviors. Complexity, 2018, 3872573
28 Lv M, Ma J, Yao Y G, et al. Synchronization and wave propagation in neuronal network under field coupling. Sci China Tech Sci, 2019, 62: 448–457
29 Parastesh F, Rajagopal K, Alsaadi F E, et al. Birth and death of spiral waves in a network of Hindmarsh-Rose neurons with exponential magnetic flux and excitable media. Appl Math Comput, 2019, 354: 377–384
30 Yan J, Zhang Q, Yin P. RNA editing machinery in plant organelles.

Sci China Life Sci, 2018, 61: 162–169
31 Wu F, Wang C, Jin W, et al. Dynamical responses in a new neuron model subjected to electromagnetic induction and phase noise. Physica A, 2017, 469: 81–88
32 Li C, Min F, Jin Q, et al. Extreme multistability analysis of memristor-based chaotic system and its application in image decryption. AIP Adv, 2017, 7: 125204
33 Chen M, Sun M, Bao B, et al. Controlling extreme multistability of memristor emulator-based dynamical circuit in flux-charge domain. Nonlinear Dyn, 2018, 91: 1395–1412
34 Chen M, Feng Y, Bao H, et al. Hybrid state variable incremental integral for reconstructing extreme multistability in memristive jerk system with cubic nonlinearity. Complexity, 2019, 8549472
35 Jafari S, Ahmadi A, Panahi S, et al. Extreme multi-stability: When imperfection changes quality. Chaos Soliton Fract, 2018, 108: 182–186
36 Njitacke Z T, Kengne J, Tapche R W, et al. Uncertain destination dynamics of a novel memristive 4D autonomous system. Chaos Soliton Fract, 2018, 107: 177–185
37 Yuan F, Deng Y, Li Y, et al. The amplitude, frequency and parameter space boosting in a memristor-meminductor-based circuit. Nonlinear Dyn, 2019, 96: 389–405
38 Bao B C, Bao H, Wang N, et al. Hidden extreme multistability in memristive hyperchaotic system. Chaos Soliton Fract, 2017, 94: 102–111
39 Bao H, Liu W, Chen M. Hidden extreme multistability and dimensionality reduction analysis for an improved non-autonomous memristive FitzHugh-Nagumo circuit. Nonlinear Dyn, 2019, 96: 1879–1894
40 Li C, Sprott J C, Mei Y. An infinite 2-D lattice of strange attractors. Nonlinear Dyn, 2017, 89: 2629–2639
41 Li C, Joo-Chen Thio W, Sprott J C, et al. Constructing infinitely many attractors in a programmable chaotic circuit. IEEE Access, 2018, 6: 29003–29012
42 Li C, Sprott J C. An infinite 3-D quasiperiodic lattice of chaotic attractors. Phys Lett A, 2018, 382: 581–587
43 Li C, Xu Y, Chen G, et al. Conditional symmetry: Bond for attractor growing. Nonlinear Dyn, 2019, 95: 1245–1256
44 Sun J, Zhao X, Fang J, et al. Autonomous memristor chaotic systems of infinite chaotic attractors and circuitry realization. Nonlinear Dyn, 2018, 94: 2879–2887
45 Strelioff C C, Hübler A W. Medium-term prediction of chaos. Phys Rev Lett, 2006, 96: 044101
46 Chen C, Chen J, Bao H, et al. Coexisting multi-stable patterns in memristor synapse-coupled Hopfield neural network with two neurons. Nonlinear Dyn, 2019, 95: 3385–3399
47 He S, Sun K, Banerjee S. Dynamical properties and complexity in fractional-order diffusionless Lorenz system. Eur Phys J Plus, 2016, 131: 254
48 Fortuna L, Baglio S, Arena P, et al. Hyperchaos from cellular neural networks. Electron Lett, 1995, 31: 250–251
49 Caponetto R, Dongola G, Fortuna L, et al. New results on the synthesis of FO-PID controllers. Commun Nonlinear Sci Numer Simul, 2010, 15: 997–1007
50 Wang N, Li C, Bao H, et al. Generating multi-scroll Chua's attractors via simplified piecewise-linear Chua's diode. IEEE Trans Circuits Syst I, 2019, doi: 10.1109/TCSI.2019.2933365
51 Buscarino A, Fortuna L, Frasca M. Experimental robust synchronization of hyperchaotic circuits. Physica D-Nonlinear Phenomena, 2009, 238: 1917–1922
52 Bao H, Wang N, Bao B, et al. Initial condition-dependent dynamics and transient period in memristor-based hypogenetic jerk system with four line equilibria. Commun Nonlinear Sci Numer Simul, 2018, 57: 264–275
53 Hua Z, Zhou Y, Bao B C. Two-dimensional sine chaotification system with hardware implementation. IEEE Trans Ind Inf, 2019, doi: 10.1109/TII.2019.2923553
54 Li C, Lin D, Lu J, et al. Cryptanalyzing an image encryption algorithm based on autoblocking and electrocardiography. IEEE MultiMedia, 2018, 25: 46–56